Targeting hypoxic prostate tumors using the novel hypoxia-activated prodrug OCT1002 inhibits expression of genes associated with malignant progression.

Heather Nesbitt[1], Niall M. Byrne[1,2], S. Nicole Williams[3], Louise Ming[1], Jenny Worthington[1,3], Rachel J. Errington[4,5], Laurence H. Patterson[6], Paul J. Smith[6], *Stephanie R. McKeown[1,6], *Declan J. McKenna[1]

[1] Biomedical Sciences Research Institute, University of Ulster, Cromore Road, Coleraine, Northern Ireland, BT52 1SA, United Kingdom

[2] Garvan Institute of Medical Research, 384 Victoria Street, Sydney, New South Wales 2010, Australia

[3] Axis Bioservices Ltd, Coleraine, Northern Ireland, BT51 3RP, United Kingdom

[4] School of Medicine, Cardiff University, Heath Park, Cardiff, CF14 4XN, United Kingdom

[5] BioStatus Ltd, Shepshed, Leicestershire LE12 9NP, United Kingdom

[6] OncoTherics Ltd, Shepshed, Leicestershire LE12 9NP, United Kingdom

* Joint senior authors

Running title: OCT1002 inhibits malignant progression of hypoxic tumours

Keywords: OCT1002, tumor hypoxia, hypoxia-activated prodrug, prostate, bicalutamide

Corresponding author: Dr Declan McKenna, Biomedical Sciences Research Institute, University of Ulster, Cromore Road, Coleraine, Northern Ireland BT52 1SA, United Kingdom. Tel: +44(0)2870124356 Fax: +44(0)2870124965 Email: dj.mckenna@ulster.ac.uk

Conflicts of interest: SR McKeown and PJ Smith are directors of OncoTherics Ltd; RJ Errington, LH Patterson and PJ Smith are directors of Biostatus Ltd.

Word count (excluding references): 5,099

Total number of figures and tables: 6 Figures

TRANSLATIONAL RELEVANCE

Tumor hypoxia is recognised as a major contributing factor in the progression of prostate cancer. This study provides the first evidence that a novel unidirectional hypoxia-activated prodrug, OCT1002, effectively targets hypoxic tumor cells; our study shows this occurs both *in vitro* and *in vivo*. In a xenograft mouse model of prostate cancer, OCT1002 improves the efficacy of the anti-androgen drug bicalutamide in controlling tumor growth. We have shown that initial treatment of androgen-sensitive tumors with bicalutamide causes vascular collapse and increased hypoxia; however, after 21 days the vasculature recovers. Our evidence shows that OCT1002 causes selective killing of tumor cells with a more malignant genotype. This provides a mechanistic explanation for why patients on hormonal therapy relapse. It also shows that targeting hypoxic tumor cells with OCT1002 offers a means by which malignant progression can be blocked in patients on androgen-deprivation therapy.

ABSTRACT

Purpose

To understand the role of hypoxia in prostate tumor progression, and to evaluate the ability of the novel unidirectional hypoxia-activated prodrug OCT1002 to enhance the anti-tumor effect of bicalutamide.

Experimental Design

The effect of OCT1002 on prostate cancer cells (LNCaP, 22Rv1, PC3) was measured in normoxia and hypoxia *in vitro*. *In vivo*, tumor growth and lung metastases were measured in mice treated with bicalutamide, OCT1002, or a combination. Dorsal skin fold chambers were used to image tumor vasculature *in vivo*. Longitudinal gene expression changes in tumors were analysed using PCR.

Results

Reduction of OCT1002 to its active form (OCT1001) decreased prostate cancer cell viability. In LNCaP-luc spheroids, OCT1002 caused increased apoptosis and decreased clonogenicity. *In vivo*, treatment with OCT1002 alone, or with bicalutamide, showed significantly greater tumor growth control and reduced lung metastases compared to controls. Re-establishment of the tumor microvasculature following bicalutamide-induced vascular collapse is inhibited by OCT1002. Significantly, the up-regulation of *RUNX2* and its targets caused by bicalutamide alone were blocked by OCT1002.

Conclusions

OCT1002 selectively targets hypoxic tumor cells and enhances the anti-tumor efficacy of bicalutamide. Furthermore, bicalutamide caused changes in gene expression which indicated progression to a more malignant genotype; OCT1002 blocked these effects, emphasising that more attention should be attached to understanding genetic changes that may occur during treatment. Early targeting of hypoxic cells with OCT1002 can provide a means of inhibiting prostate tumor growth and malignant progression. This is of importance for the design and refinement of existing androgen-deprivation regimens in the clinic.

INTRODUCTION

Hypoxia occurs in most solid tumors and it is known to have a major influence on treatment response to both radiotherapy (1) and chemotherapy (2). Untreated prostate tumors are no exception and they have been found, in several studies, to have very low median oxygen levels (2.4mmHg; 0.3% oxygen)(3, 4), which is >12 times lower than oxygen levels found in the normal prostate (30 mmHg; 3.9% oxygen)(5). Studies have shown that high levels of hypoxia significantly correlate with increasing clinical stage and can predict biochemical failure following radiotherapy (6). Importantly, hypoxia has also been implicated as a causative factor in malignant progression, with many effects mediated through increased expression of HIF-1 (7). In addition, hypoxia has been shown to cause genetic instability (8), gene amplification (9), endothelial to mesenchymal transition (EMT)(10, 11) and the selection of cells with diminished apoptotic potential and a greater invasive potential (12-15). Hypoxia is therefore a significant impediment to the successful outcome of many cancer treatments.

One approach to blocking the influence of hypoxic tumor cells is to directly target this sub-population with a hypoxia-activated prodrug (HAP); these prodrugs are a diverse group of chemicals that can be reduced in cells when oxygen levels are very low (16, 17). The majority of HAPs are reduced in single-electron reduction steps, a process which is reversible when oxygen levels increase and is associated with superoxide formation. In contrast, alkylaminoanthraquinone di N-oxides are irreversibly reduced by addition of two electrons on each of the two N-oxide side arms of the anthraquinone ring. This results in formation of metabolically stable reduction products; for this reason it is proposed they should be classified separately as unidirectional HAPs (uHAPs). Currently there are two compounds of therapeutic interest presenting these advantageous properties, namely AQ4N (18) and a recently described deuterated analogue OCT1002 (OncoTherics Ltd)(19). Under tumor-relevant hypoxic conditions the two sequential $2e^-$ reductions yield the toxic metabolites AQ4 and OCT1001 respectively (5). These stable reduction products have very high affinity for DNA and they also target topoisomerase II (20), which can effect a long-term inhibition of both DNA replication and cell cycle traverse (21). OCT1002 is distinguished from AQ4N by its highly selective deuterium substitution of the 12 hydrogen atoms contained within the two N-oxide side chains (22). Deuteration can modify the rate of cleavage of covalent bonds to deuterium, creating a deuterium kinetic isotope effect, slowing cytochrome P450 metabolism of the deuterated versions of drug candidates (23).

Further, non-covalent interactions between molecules can be modified by deuteration (24), while differences in the polarities of deuterated versus non-deuterated isomers can potentially alter the complex subcellular localization and sequestration properties (25) and contribute to an enhanced intracellular persistence of the activated drug OCT1001 (19).

To test the effectiveness of these uHAPs *in vivo*, we routinely utilise a murine LNCaP-luc xenograft model of prostate cancer in our laboratory (11, 26). This is an ideal system to investigate tumor hypoxia, since LNCaP/LNCaP-luc tumors have a low oxygen level (~6mm Hg; 0.8% oxygen) comparable to that observed in patients. Furthermore, we have used this model to demonstrate that this level falls even further to about 0.1% oxygen upon initiation of bicalutamide treatment, due to vascular collapse (26). Bicalutamide is a widely used drug used in androgen deprivation therapy (ADT) and provides for effective control of locally advanced prostate cancer prostate tumors. However remissions normally last only about 18-24 months before tumors recur, often as the more highly metastatic castrate resistant prostate cancer (CRPC)(27). Our previous results led us to hypothesise that the bicalutamide-induced hypoxia may select for cells with a more aggressive phenotype, a selection which we subsequently demonstrated was characterised by up-regulation of several pro-survival genes and a promotion of the EMT phenotype (11). Notably, when a single dose of uHAP (AQ4N) was administered during the bicalutamide-induced hypoxic phase in this model, tumor growth was significantly delayed (26). In the current study, we have investigated if a similar growth delay occurs in the same xenograft model when OCT1002 is used alone and in combination with bicalutamide. We also profile genetic changes in response to both bicalutamide and OCT1002 treatment to determine if bicalutamide-induced alterations in genes associated with metastatic progression were blocked by the use of OCT1002.

MATERIALS AND METHODS

Cell Culture

All cell-lines were obtained from American Type Culture Collection (ATCC, Rockville, MD, USA). Cells were frozen at low passage number and used within 3-6 passages after thawing. Cells were authenticated by in-house genotyping service and routinely tested as mycoplasma-free (InvivoGen, Toulouse, France). A luciferase-expressing variant of the parental LNCaP cells was developed and confirmed to have similar characteristics to the parental cells (26). These LNCaP-luc cells were cultured in RPMI 1640 culture medium (Life Technologies, Paisley, UK) supplemented with 10% foetal bovine serum (FBS), D-glucose (10mM; Sigma, Poole, UK) and HEPES (10mM; Sigma). PC3 and 22Rv1 were cultured in RPMI-1640 supplemented with 10% FBS. For OCT1002 treatment, 5,000 cells were seeded in a 96 well plate and allowed to adhere overnight. Cells were treated with OCT1002 (10^{-12} to 10^{-3}M in vehicle) at 37°C. After 72 hours, a cell viability XTT assay (Roche, Sussex, UK) was carried out. For treatment in hypoxic conditions, 5,000 cells were seeded in a 96 well plate and allowed to adhere overnight. After dosing with OCT1002 (1µM), cells were placed in normoxia (20% oxygen) or hypoxia (0.1% oxygen) at 37°C in a hypoxia work station (Ruskinn Technology, UK) for up to 48 hours: cell viability was measured using a XTT assay.

Spheroid 3D cell culture

5,000 LNCaP-luc cells were seeded in non-adherent 24 well plates and spheroids allowed to form upon continued incubation. On Day 7, spheroids were treated with vehicle (0.1% DMSO), bicalutamide (13.8 µM), OCT1002 (1 µM) or bicalutamide + OCT1002. Spheroid growth was measured at Day 4, 6, 8, 10, 11 and 12. Images were taken at 100X magnification. For colony forming assays, spheroids were collected by centrifugation on Day 10, re-suspended as a single cell suspension and seeded on adherent 6 well plates. After 7 days, colonies were fixed and stained with crystal violet (2%). Quantification was performed by addition of 0.1% SDS to the wells and absorbance was measured at 595nm. Spheroids, treated on Day 4, were disaggregated and stained 72 hours later with an Annexin/PI apoptosis kit (Life Technologies) and analysed by flow cytometry on a Gallios™ Flow Cytometer (Beckman-Coulter, High Wycombe, UK).

Quantitative Real-Time PCR

RNA was extracted from spheroids using Trizol® (Life Technologies) and cDNA prepared using RevertAid reagents (Fermentas, Cambridge, UK). Quantitative Real-Time PCR (qPCR) was carried out using SYBR green (Fermentas) and gene specific primers (Supplementary Table S1) on a LC480 Lightcycler (Roche).After normalization to the reference gene(s), relative expression levels of each target gene were calculated using the comparative C_T ($\Delta\Delta CT$) method. qPCR for miR-210 was performed using the miRCURY LNA™ microRNA PCR system (Exiqon, Vedbaek, Denmark) using 20ng template RNA. PCR was performed on the LC480 Lightcycler, normalization was against U6snRNA and relative expression levels calculated using the comparative C_T ($\Delta\Delta CT$) method. All PCR graphs represent the combined results from ≥3 independent biological replicates, unless otherwise indicated.

Western Blotting

Protein was extracted from spheroids using urea buffer. Primary antibodies used were obtained from Cell Signaling Technology unless otherwise stated and comprised: PARP/Cleaved PARP (#9542, 1:1000), Bax (#2772S, 1:500), Bcl-2 (#2876S,1:500), β-actin (#4967,1:1000) and GAPDH (Millipore, ABS16,1:1000). Membranes were blocked in 5% BSA diluted in 1x TBS-T (0.05%) followed by incubation in the appropriate secondary antibody (goat anti-rabbit IgG-HRP (1:10000) or goat anti-mouse IgG-HRP (1:10000)). Secondary antibodies were purchased from Santa Cruz Biotechnology (Heidelberg, Germany).

***In vivo* methods**

Animal maintenance. In vivo experiments were conducted in accordance with the Animal (Scientific Procedures) Act 1986 and the UKCCCR guidelines for the welfare of animals in experimental neoplasia (28). 8-10 week old male BALB/c immune-compromised (SCID) mice weighing 25-30g (Envigo, Cambridgeshire, UK) were housed under standard laboratory conditions in a temperature controlled (22°C; 50-55% humidity) pathogen free environment with a 12 hour light-dark cycle. Food and water was supplied *ad libitum*. All surgical procedures were performed under aseptic conditions and the body temperature of animals was kept constant using heated pads.

Xenograft establishment and tumor growth delay. LNCaP-luc or 22Rv1 xenografts were established on the dorsum of SCID mice by subcutaneous injection of 2×10^6 cells suspended in 100µl of matrigel with a 21g needle (Becton Dickinson, Oxford, UK). Once the tumor became palpable dimensions were measured using Vernier calipers.

Drug administration. Bicalutamide was prepared in vehicle (0.1% DMSO in corn oil)(Sigma) and administered orally (p.o.) via gavage as 2mg/kg daily. OCT1002 (OncoTherics, Shepshed, UK) was prepared in sterile phosphate buffered saline (PBS) and administered as a single intraperitoneal (i.p.) injection (50mg/kg). When tumor volume reached between 100–150mm^3, mice were randomly assigned to treatment groups and dosing initiated. Animals were sacrificed at day 28 or when tumor reached the maximum size permitted.

Assessment of metastasis. Upon Day 28 animals were injected i.p. with D-Luciferin (150 mg/kg in PBS) 5 min prior to imaging. Animals were sacrificed, lungs were removed to detect bioluminescence using the IVIS imaging system (Xenogen, Santa Clara, CA). Within a region of interest the total light flux (photons/second) was measured.

Dorsal skin fold model

Dorsal skin fold (DSF) preparation. A bespoke transparent DSF 'window chamber' (APJ Trading Co. Ltd, USA) was attached to the dorsum of mice as previously described (26, 29). This consisted of a titanium frame with a viewing port into which a tumor fragment was placed. The DSF preparation was then hydrated with sterile saline and closed with a glass coverslip secured by a spring c-clip.

Imaging of treatment-induced changes in the tumor vasculature. The tumor fragment was left in place for one week to allow vascularisation. Bicalutamide treatment was then initiated (day 0). Five minutes prior to imaging (days 0. 7, 14 and 21) mice were given 50µl 150 kDa fluorescein isothiocyanate-labeled (FITC) dextran (50mg/ml in saline)(Sigma) into the tail vein. Mice were secured in a bespoke restraint and placed laterally onto a modified microscope stage. Tumor microvessels were imaged using a HC PL APO lens (10X magnification) fitted to a TCS SP5 confocal microscope (Leica Microsystems, Germany). Three random regions of interest (ROIs) were identified at various locations within each tumor and consecutive images were taken. At each ROI image stacks were created through the z-plane of the tumor tissue with a final maximum projection created using the

Leica application suite advanced fluorescence (LAS AF®) software. Images were analysed offline using ImageJ software (National Institute of Mental Health, Maryland, USA) and stereological analysis performed using a Merz grid (30). Visualization of OCT1002 was performed 4 h after drug administration with a helium neon laser (excitation at 633nm; emission 650nm–800 nm). Images were subsequently merged with FITC-dextran labelled tumor vasculature.

PCR custom array gene expression analysis

5µg RNA per tumor sample was reverse transcribed using RevertAid[TM] (Fermentas) and cDNA from 3 tumors per treatment on specific days (0, 7, 14, 21 and 28) were pooled. Changes in expression profile were analysed on RealTime Ready custom 96 well panels (Roche)(Supplementary Figure S1). PCR was performed on the LC480 lightcycler and results were normalised to reference genes (HPRT, beta actin and 18s ribosomal RNA). Fold changes in gene expression of vehicle and bicalutamide treated xenografts were compared to pre-treatment (Day 0) expression levels; genes considered up-regulated (≥2) or down-regulated (≤0.5) and those which satisfied a p value <0.05 (student t-test) were deemed statistically significant.

Immunohistochemistry

Tumors at the experimental endpoint were excised, fixed in PFA and wax-embedded. 5µM sections were stained with RUNX2 (27-K, 1:50), ki-67 (SP6, 1:100) and IgG antibodies (all Santa Cruz Biotechnology) using Superpicture 3rd Gen IHC kit (Life Technologies). Five fields per sections were viewed, scored and averaged. Immunohistochemistry staining was scored using a two approach method for extent and intensity (31). Extent of staining was defined as the percentage of cells with nuclear immunoreactivity and was scored 0-5: negative (0); ≤10% (1); 11%–25% (2); 26%–50% (3); 51%–75% (4) and ≥76% (5). Intensity of staining was scored 0-5: negative (0)-very strong (5). Scores were averaged with 3 mice per group.

Statistical analysis

Data from qPCR analyses and tumor growth delay studies were analysed using a two-tailed student's t-test. All remaining datasets were analysed using a two-way ANOVA with Bonferroni post-test

analysis. All statistical analysis was carried out using the Prism 5.0 software (GraphPad). Differences between points were deemed statistically significant with a $p < 0.05$ (95% confidence interval).

RESULTS

Novel uHAP OCT1002 is reduced to active form OCT1001 in hypoxic conditions

OCT1002 is electrically neutral in aqueous solution but in hypoxic tumor cells it can be reduced to the DNA-affinic cytotoxin OCT1001 (Figure 1A). Imaging 4 hours after OCT1002 administration on Day 7 showed extensive distribution of drug far-red fluorescence (19) in the tumor, particularly in the more hypoxic centre (Figure 1B). When the tumors were imaged 7 days later the bound drug is still clearly visible, particularly away from blood vessels, confirming the longevity of OCT1001 in hypoxic cells. No autofluorescence was seen in untreated tumor fragments (Figure 1B).

Activated OCT1002 targets hypoxic cells *in vitro*

Treatment of 3 prostate cancer cell-lines (LNCaP-luc, 22Rv1, PC3) at a range of OCT1002 concentrations (10^{-12} to 10^{-3}M) revealed no significant toxicity at concentrations of <1μM (Figure 1C). When LNCaP-luc cells were grown in hypoxic conditions (0.1%) for 48 hours, there was an expected decrease in cell viability (Figure 1D) compared to cells grown in normoxic conditions (20%). However, treatment of these hypoxic cells with 1μM OCT1002 resulted in a further significant decrease in the viability of the cells (Figure 1D, grey bars). In contrast, OCT1002 treatment of cells grown in normoxic conditions had no effect (Figure 1D, white bars), indicating that the drug only targets cells in hypoxic conditions. Similar results were obtained for both 22Rv1 and PC3 cells (Supplementary Figure S2).

We also utilised a 3D spheroid model of prostate cancer growth to illustrate the effect of OCT1002 on hypoxic LNCaP-luc cells. The increasing presence of hypoxia in growing spheroids was confirmed by the increasing levels of the hypoxic markers IGF1 and miR-210 (Figure 2A) and HIF1α protein (Figure 2B). Again, the prevalence and localisation of hypoxia-activated OCT1001 in the spheroids could be detected in the far-red spectral window (Figure 2B, images). The developing hypoxia occurs concurrently with an increase in spheroid size over a 10 day period. Addition of bicalutamide on Day 7 significantly attenuated their growth and an even greater decrease in spheroid growth and reduction in size was found when OCT1002 was added (Figure 2C). Upon disaggregation, the ability of both bicalutamide- and OCT1002-treated spheroids to form colonies was significantly decreased in comparison to untreated spheroids (Figure 2D). In spheroids treated with OCT1002 there was a

significant increase in the number of apoptotic cells (Figure 2E, Supplementary Figure S3A). This was consistent with the concomitant decrease in Bcl-2 protein levels and increase in Bax protein levels, as well as evidence of PARP cleavage (Supplementary Figure S3B). Taken together, we conclude that OCT1002 is indeed activated in hypoxic conditions *in vitro*, resulting in increased cell death.

OCT1002 in combination with bicalutamide improves tumor growth control and reduces lung metastases

The LNCaP-luc xenograft mouse model of prostate tumorigenesis was used to measure the effect of OCT1002 *in vivo* (Figure 3A and 3B). Tumor growth was measured during treatment with 2mg/kg bicalutamide; although it initially slowed growth by Day 28 the tumor growth delay (1.09±0.55 days) was not significantly different from that found in the vehicle-treated group. OCT1002 was administered as a single low dose (50mg/kg) on Day 7, which we had previously confirmed as the hypoxic nadir following bicalutamide treatment. When given with vehicle, OCT1002 caused a moderate delay in tumor growth (3.88±0.56 days). However, when OCT1002 was combined with bicalutamide there was a very significant increase in tumor growth delay (22.24±5.17 days). This effect was significantly different from both vehicle-only and bicalutamide-only tumors from Day 16 until the end of the experiment (Day 28). By Day 28, vehicle-treated mice had significant metastatic spread to the lungs (Figure 3C). Although bicalutamide-treated mice had a slightly reduced level of lung metastasis this was not significant, whereas OCT1002 in combination with bicalutamide significantly reduced metastatic spread by ~10 fold (Figure 3D). When a similar experiment was performed in a 22Rv1 xenograft model, the combination of OCT1002 and bicalutamide in this model also resulted in greater tumor growth control (Supplementary Figure S4).

Effect of bicalutamide on vascular density is abrogated by OCT1002

As previously (26) we used a DSF preparation to evaluate the effect of drug treatments on tumor vasculature (Figure 4A–4D, Supplementary Figure S5). Vehicle-treated tumors showed little or no change in vasculature over time. Treatment with a single dose of OCT1002 (50mg/kg) on Day 7 caused a reduction in tumor microvessels when imaged on Days 14 and 21 (Figure 4A). Treatment

with daily bicalutamide reduced the microvessel density (MVD) by half when measured on Day 7, with further loss by Day 14, yet a marked vascular recovery was evident by Day 21 (Figure 4A), consistent with our previous studies (11, 26). Data from window chamber experiments on 22Rv1 tumors also showed bicalutamide-induced hypoxia and concomitant changes in vasculature similar to that observed for LNCaP tumors (Supplementary Figure S6). Notably, in LNCaP xenografts, OCT1002 administered on Day 7 blocked the re-establishment of microvessels seen after 21 days of bicalutamide treatment (Figure 4A). Quantification of the vascular coverage at Day 21 showed administration of OCT1002, alone or in combination with bicalutamide, resulted in reduced MVD and fewer branch points compared to vehicle or bicalutamide alone (Figure 4B and 4C). Conversely, as expected, vessel length was increased in the presence of OCT1002, as the microvascular network was not re-established unlike that observed in bicalutamide-treated mice (Figure 4D). Full stereological measurements from Day 0-21 are shown in Supplementary Figure S5, demonstrating that the re-vascularisation that occurs at Day 21 with bicalutamide treatment is blocked when OCT1002 is present.

OCT1002 modifies bicalutamide-induced changes in gene expression

qPCR arrays were used to compare longitudinal changes in expression of 70 genes in tumors during treatment. Expression changes for all genes are shown as scatter plots (Figure 5A). Genes were significantly different if they fell to the left of the vertical line and above or below the horizontal lines (student *t*-test). Expression of most genes changed at some time during the 28 days showing that treatment caused complex changes in the overall genetic profile. Notably, at Day 21, the significant up-regulation of many genes induced by bicalutamide treatment is not observed when bicalutamide is combined with OCT1002. More detailed examination of the variations in gene expression on Day 21 revealed that the genes highlighted by filtering analysis are involved in promoting cell survival. Notably, the induction of these genes at Day 21 in response to bicalutamide was ablated by addition of OCT1002 (Figure 5B).

Expression of *RUNX2* and pro-survival genes induced by bicalutamide is blocked by OCT1002

Significantly, one of these was *RUNX2*, which regulates expression of several targets involved in pro-survival pathways and which we had previously noted as important in the hypoxic stress response (32, 33). Immunohistochemistry revealed that addition of OCT1002 significantly reduced the expression of RUNX2 protein, as well as Ki67 staining, in LNCaP-luc tumors (Figure 6A). Furthermore, when we examined the expression of *RUNX2* and several of its downstream targets, in our LNCaP-luc spheroid model, we also found that OCT1002 blocked the bicalutamide-induced up-regulation of these genes (Figure 6B).

DISCUSSION

Understanding the physiological and molecular characteristics of the tumor microenvironment before, during and after treatment is crucial in developing and improving therapies for prostate cancer (34). In particular, the effect of hypoxia upon tumor progression is a key consideration, since it has been consistently associated with an increasingly malignant phenotype. (12-15). In our studies, we have used a mouse LNCaP-luc xenograft model of prostate cancer; this provided an ideal method for monitoring genetic and physiological changes longitudinally. It enabled us to examine how targeting hypoxic tumor cells with the novel uHAP, OCT1002, can improve the anti-tumor efficacy of bicalutamide.

As OCT1002 is a new agent, it was first necessary to confirm that the prodrug was converted to the active form (OCT1001) in hypoxic tumors. We have shown that the drug penetrated throughout tumor fragments grown in window chambers and that it remained in the reduced form for some considerable time (>7 days)(Figure 1A and 1B). Since most of the prodrug will have been eliminated after 4 hours (half-life about 45–60 mins in mice), the fluorescent signal reflects only the highly DNA-affinic reduction product OCT1001 which is bound in hypoxic cells. We then showed that OCT1002 at high concentrations ($>10^{-6}$M) showed cytotoxicity against 3 prostate cancer cell monolayers and that OCT1002 could target hypoxic prostate cells more effectively in hypoxia (0.1%)(Figure 1C and 1D, Supplementary Figure S2). This confirms additional studies we have carried out showing an oxygen-dependent enhancement of cytotoxicity in a range of other cell lines (data not shown). We also used LNCaP-luc spheroids to more closely recapitulate *in vivo* tumor formation, since hypoxia develops as the spheroid grows (Figure 2A-2C). We show that this spheroid hypoxia reduces OCT1002 and results in significant cell death, evidenced by reduced spheroid size and increased apoptotic markers. Furthermore, spheroids had significantly reduced ability to form colonies after treatment with OCT1002 as compared to controls (Figure 2D). This suggests that specifically killing hypoxic cells reduces viable clonogens, which may be crucial for reducing cells with metastatic potential *in vivo*. Flow cytometry suggests that OCT1002 promotes apoptosis, whereas bicalutamide induces more necrosis, presumably due to the differing modes of action of these drugs (Figure 2E). However, the combination of these agents needed to be explored in vivo to better assess how they would impact upon tumor growth in a more complex microenvironment.

Previously we have shown that bicalutamide treatment (2-6mg/kg daily) caused immediate severe hypoxia in LNCaP-luc xenografts over 1-14 days due to vascular collapse which slowly recovered over the next 14 days (11, 26). Hence we have now examined the effect of the novel uHAP, OCT1002, on this effect by administration of a single low dose of OCT1002 (50mg/kg) at the hypoxic nadir (Day 7). In combination with daily bicalutamide there was a significant slowing of tumor growth; this effect was observed up to the end of the experiment (Day 28), indicating that targeting hypoxic cells can enhance the anti-tumor effect of bicalutamide for some considerable time. Interestingly, treatment with OCT1002 alone also proved to be slightly more effective in controlling tumor growth than bicalutamide treatment alone. Presumably this is because it is activated by the inherently hypoxic tumor environment (5), even without the extra hypoxia induced by bicalutamide effect on the vasculature. Notably, OCT1002 significantly inhibited metastatic spread to the lungs, suggesting that targeting hypoxic cells also targets cells with increased metastatic potential.

In the absence of another reliable androgen-sensitive xenograft model to validate our results, we investigated 22Rv1 xenografts. However, these tumors are very hematogenous, grow very fast *in vivo* and respond only slightly to bicalutamide. Nonetheless, bicalutamide caused marked losses in microvessels and profoundly reduced oxygenation, consistent with the effect in LNCaP tumors (Supplementary Figure S6). When OCT1002 was combined with bicalutamide there was improved growth control in 22Rv1 tumors (Supplementary Figure S4), suggesting that OCT1002 activation was improved when administered during the period of bicalutamide-induced hypoxia. Interestingly, the bicalutamide-treated tumors became less hematogenous and easier to work with, perhaps due to the anti-vascular effects of the bicalutamide. Even so, 22Rv1 tumors are more challenging to work with *in vivo* than LNCaP tumors and provide, in our opinion, a model which is of limited value for comparison with androgen-sensitive slow-growing human tumors. Even moderate-sized tumors start to deteriorate and we would urge caution at using 22Rv1 cells as xenografts. Nevertheless, our data shows that a single moderate dose of OCT1002 produced significant anti-tumor effects, providing further pre-clinical evidence of the potential of OCT1002 in the treatment of prostate cancer.

It is also notable that OCT1002 prevents the revascularisation observed during bicalutamide treatment in LNCaP-luc xenograft tumors, suggesting that the cells responsible for driving the vascular recovery are also inhibited or killed by OCT1002 (Figure 4, Supplementary Figure S5). This

data is particularly pertinent since several chemotherapeutic drugs have also been shown to cause tumor shrinkage and vascular collapse, with a corresponding reduction in oxygen levels, even when if this is not directly linked to the mechanism of action of the drugs (35-37). This hypoxic stress could provide an environment which selects for cells with increased metastatic potential that survive to repopulate the tumor, implying that a combination of therapies are required to prevent progression to a more malignant tumor. This was also the conclusion of another recent study which suggested that combination of ADT with inhibitors that block hypoxia-induced chemokine production may prevent emergence of CPRC in a mouse metastatic prostate (TRAMP) model (38). In humans, this concept may explain recent results from a large clinical trial that showed using docetaxel in addition to ADT improved relapse-free survival in patients with high-risk localised prostate cancer (39). Docetaxel would have added cytotoxic effect to the growth-slowing effect of bicalutamide, increasing the total cell kill and therefore prolonging the time to relapse. Similarly, this may also explain why widespread clinical testing of drugs which directly target tumor angiogenesis have not provided the panacea that was expected, perhaps because they drive hypoxic selection of more malignant cells, which survive to resist further treatment (40). Indeed, the LNCaP xenograft model presented here would be ideal for studying effects of other commonly used prostate cancer drugs, such as enzalutamide and abiraterone, to investigate this phenomenon further and to help inform clinical practice.

We were also interested to see how OCT1002 would impact upon gene expression patterns that we have previously investigated in profiling the response to bicalutamide treatment alone (11). We screened a set of 70 genes at each time-point in the treatment groups and filtered the data to identify genes which were consistently and significantly altered (Figure 5A). We focused on results from Day 21, since we expected the hypoxic stress at this time to be reflected in the gene signatures within the tumors. We noted that bicalutamide treatment induced an up-regulation in a large number of genes at Day 21 in response to the severe hypoxia. However, this was largely absent at this time-point when OCT1002 was combined with bicalutamide. Further examination of the genes affected at Day 21 (Figure 5B), showed that they reflected genes involved in promoting cell survival through various mechanisms such as angiogenesis, transcription, adhesion, invasion, apoptosis and cell cycle maintenance. Notably, the induction of almost all these genes at Day 21 in response to bicalutamide was ablated by addition of OCT1002 (Figure 5B). These results support our proposal above that some cells can survive the bicalutamide-induced hypoxia and that this is linked to up-regulation of an

array of pro-survival genes, which help re-establish the tumor vasculature. Ultimately, this could result in the hypoxia-driven selection of cells which exhibit a more aggressive, malignant phenotype. Worryingly, this suggests that bicalutamide use in patients may in fact increase prostate cancer tumor hypoxia soon after treatment, thereby selecting for cells which have increased metastatic potential. Our data corroborates previous studies of prostate cancer cells which have shown that hypoxia can indeed select for cells with a more malignant genotype/phenotype (13, 41, 42), with several reports detailing the up-regulation of various genes in response to hypoxic insult, including those associated with a pro-angiogenic phenotype (43), stem cell maintenance (44), genetic instability (8), protection from apoptosis (45) and malignant progression (15). With this in mind, it is significant that the up-regulation of pro-survival genes is not observed at Day 21 when the OCT1002 is combined with bicalutamide. This indicates that the cells which survive the hypoxic insult, and subsequently alter gene expression, are targeted and killed, which is evidenced in increased tumor growth control.

We have previously highlighted the link between hypoxic stress and *RUNX2* (32, 33), so we were interested to see that induction of *RUNX2* expression by bicalutamide treatment was effectively blocked by OCT1002 exposure. This is significant because *RUNX2* expression is up-regulated in prostate (46), breast (47, 48) and colon cancer (49) and is thought to contribute to a more aggressive, metastatic phenotype by altering expression of many genes involved in migration, invasion, metastasis, apoptosis and angiogenesis (32, 46, 49). Similarly, in this study, the induction of *RUNX2* correlated with induction of several of its downstream targets (Figure 6A). However, when OCT1002 was added to a bicalutamide treatment, the induction of *RUNX2* and the associated targets was not observed, even though a significant hypoxic stress still existed in these tumors given that the vasculature had not been restored. Confirmation of this effect was found when we examined *RUNX2* expression and other genes in our spheroid model (Figure 6B). This corroborates our previous work which proposes *RUNX2* is a key regulator in helping cells survive the hypoxic stress. Our study suggests that the addition of OCT1002 targets those cells, thereby preventing *RUNX2* up-regulation and subsequently the development of more aggressive tumor cells. Our proposed model is shown in Figure 6C, wherein the hypoxic-resistant cells within the heterogenous tumor cell population survive to repopulate the tumor, leading to relapse and CPRC development. However, addition of OCT1002 targets these cells, preventing regrowth of the microvasculature in particular and thereby exerting

greater tumor growth control. Future work will further characterise the exact role of RUNX2 and other key molecular changes during this process.

Conclusions

In conclusion, this study shows that the novel uHAP OCT1002 effectively targets hypoxic prostate cancer cells and improves the ability of bicalutamide to control growth of human prostate tumours in mice We propose that the enhanced efficacy is due to selective killing of cells that would otherwise survive the severe hypoxic conditions induced by vascular collapse soon after initiation of bicalutamide treatment. Since the genes up-regulated during bicalutamide treatment are predominantly pro-survival, we hypothesise that these cells survive to establish a tumor with a more malignant phenotype; this may help explain why patients treated solely with ADT exhibit a relatively early relapse. However, our data suggests that inclusion of OCT1002 at the early stage of the ADT regimen to eliminate hypoxic cells could provide a method for eradication of the more malignant hypoxic cell population. Our data provides increased understanding of the physiological and molecular changes in the prostate cancer microenvironment that occur during treatment and we suggest that more awareness of these changes should be taken into account when deciding on ADT schedules for prostate cancer patients.

REFERENCES

1.   Moeller BJ, Richardson RA, Dewhirst MW. Hypoxia and radiotherapy: opportunities for improved outcomes in cancer treatment. Cancer Metastasis Rev 2007;26:241-8.

2.   Rohwer N, Cramer T. Hypoxia-mediated drug resistance: novel insights on the functional interaction of HIFs and cell death pathways. Drug Resist Updat 2011;14:191-201.

3.   Movsas B, Chapman JD, Hanlon AL, Horwitz EM, Pinover WH, Greenberg RE, et al. Hypoxia in human prostate carcinoma: an Eppendorf PO2 study. Am J Clin Oncol 2001;24:458-61.

4.   Milosevic M, Chung P, Parker C, Bristow R, Toi A, Panzarella T, et al. Androgen withdrawal in patients reduces prostate cancer hypoxia: implications for disease progression and radiation response. Cancer Res 2007;67:6022-5.

5.   McKeown SR. Defining normoxia, physoxia and hypoxia in tumors-implications for treatment response. Br J Radiol 2014;87:20130676.

6.   Turaka A, Buyyounouski MK, Hanlon AL, Horwitz EM, Greenberg RE, Movsas B. Hypoxic prostate/muscle PO2 ratio predicts for outcome in patients with localized prostate cancer: long-term results. Int J Radiat Oncol Biol Phys 2012;82:e433-9.

7.   Semenza GL. Cancer-stromal cell interactions mediated by hypoxia-inducible factors promote angiogenesis, lymphangiogenesis, and metastasis. Oncogene 2013;32:4057-63.

8.   Bristow RG, Hill RP. Hypoxia and metabolism. Hypoxia, DNA repair and genetic instability. Nat Rev Cancer 2008;8:180-92.

9.   Taiakina D, Dal Pra A, Bristow RG. Intratumoral hypoxia as the genesis of genetic instability and clinical prognosis in prostate cancer. Adv Exp Med Biol 2014;772:189-204.

10.   Jiang J, Tang YL, Liang XH. EMT: a new vision of hypoxia promoting cancer progression. Cancer Biol Ther 2011;11:714-23.

11.   Byrne NM, Nesbitt H, Ming L, McKeown SR, Worthington J, McKenna, DJ. Androgen deprivation in LNCaP prostate tumor xenografts induces vascular changes and hypoxic stress resulting in promotion of epithelial to mesenchymal transition. Br J Cancer 2016;114:659-68.

12. Graeber TG, Osmanian C, Jacks T, Housman DE, Koch CJ, Lowe SW, et al. Hypoxia-mediated selection of cells with diminished apoptotic potential in solid tumors. Nature 1996;379:88-91.

13. Butterworth KT, McCarthy HO, Devlin A, Ming L, Robson T, McKeown SR, et al. Hypoxia selects for androgen independent LNCaP cells with a more malignant geno- and phenotype Int J Cancer 2008;123:760-8.

14. Rudolfsson SH, Bergh A. Hypoxia drives prostate tumor progression and impairs the effectiveness of therapy, but can also promote cell death and serve as a therapeutic targets. Expert Opin Ther Targets 2009;13:219–25.

15. Tsai YP, Wu KJ. Hypoxia-regulated target genes implicated in tumor metastasis. J Biomed Sci 2012;19:102.

16. McKeown SR, Cowen RL, Williams KJ. Bioreductive drugs: from concept to clinic. Clin Oncol (R Coll Radiol) 2007;19:427-42.

17. Guise CP, Mowday AM, Ashoorzadeh A, Yuan R, Lin WH, Wu DH, et al. Bioreductive prodrugs as cancer therapeutics: targeting tumor hypoxia. Chin J Cancer. 2014;33:80-6.

18. Patterson LH. Bioreductively activated antitumor N-oxides: the case of AQ4N, a unique approach to hypoxia-activated cancer chemotherapy. Drug Metab Rev 2002;34:581-92.

19. Smith PJ, Wiltshire M, Nesbitt H, Byrne N, Ming L, McKenna DJ, et al. Cytometry of Anticancer Prodrug OCT1002 Activation and Targeting Using In Vitro and In Vivo Models of Tumor Hypoxia. In: CYTO 2015, the 30th Congress of the International Society for Advancement of Cytometry; Glasgow, Scotland. 2015; ISAC:268.

20. Smith PJ, Blunt N, Desnoyers R, Giles Y, Patterson LH. DNA topoisomerase II-dependent cytotoxicity of alkylaminoanthraquinones and their N-oxides. Cancer Chemother Pharmacol 1997;39:455-61.

21. Fox ME, Smith PJ. Long-term inhibition of DNA synthesis and the persistence of trapped topoisomerase II complexes in determining the toxicity of the antitumor DNA intercalators mAMSA and mitoxantrone. Cancer Res 1990;50:5813-8.

22. Ogrodzinski SS, Smith PJ, McKeown S, Patterson LH, Errington RJ. New compounds and uses thereof. In: USPTO, editors. Vol. US 2015/0307441 A1. Biostatus Ltd, Shepshed, Leicestershire, GB, 2015.

23. Shao L, Hewitt MC. The kinetic isotope effect in the search for deuterated drugs. Drug News Perspect 2010;23:398-404.

24. Wade D. Deuterium isotope effects on noncovalent interactions between molecules. Chem Biol Interact 1999;117:191-217.

25. Smith PJ, Desnoyers R, Blunt N, Giles Y, Patterson LH, Watson JV. Flow cytometric analysis and confocal imaging of anticancer alkylaminoanthraquinones and their N-oxides in intact human cells using 647-nm krypton laser excitation. Cytometry 1997;27:43-53.

26. Ming L, Byrne NM, Camac SN, Mitchell CA, Ward C, Waugh DJ, et al. Androgen deprivation results in time-dependent hypoxia in LNCaP prostate tumors: informed scheduling of the bioreductive drug AQ4N improves treatment response. Int J Cancer 2013;132:1323-32.

27. Shen M, Abate-Shen C. Molecular genetics of prostate cancer: new prospects for old challenges Genes Dev 2010;24:1967–2000.

28. Workman P, Aboagye EO, Balkwill F, Balmain A, Bruder G, Chaplin DJ, et al. Guidelines for the welfare and use of animals in cancer research. Br J Cancer 2010;102:1555–77.

29. O'Rourke M, Ward C, Worthington J, McKenna J, Valentine A, Robson T, et al. Evaluation of the antiangiogenic potential of AQ4N. Clin Cancer Res 2008;14:1502-9.

30. Howard CV and Reed MG. Unbiased Stereology. Three Dimensional Measurement in Microscopy. Abingdon: Garland Science; 2nd edition; 2005.

31. Braconi C, Bracci R, Bearzi I, Bianchi F, Sabato S, Mandolesi A, et al. Insulin-like growth factor (IGF) 1 and 2 help to predict disease outcome in GIST patients. Ann Oncol 2008;19:1293-8.

32. Browne G, Nesbitt H, Ming L, Stein GS, Lian JB, McKeown SR, et al. Bicalutamide-induced hypoxia potentiates RUNX2-mediated bcl-2 expression resulting in apoptosis resistance. Br J Cancer 2012;107:1714-21.

33. Nesbitt H, Browne G, O'Donovan KM, Byrne NM, Worthington J, McKeown SR, et al. Nitric Oxide Up-Regulates RUNX2 in LNCaP Prostate Tumors: Implications for Tumor Growth In Vitro and In Vivo. J Cell Physiol 2016;231:473-82.

34. Junttila MR, de Sauvage FJ. Influence of tumor micro-environment heterogeneity on therapeutic response. Nature 2013;501:346-54.

35. Casanovas O, Hicklin DJ, Bergers G, Hanahan D. Drug resistance by evasion of antiangiogenic targeting of VEGF signaling in late-stage pancreatic islet tumors. Cancer Cell 2005 8:299-309,

36. Wilson C, Scullin P, Worthington J, Seaton A, Maxwell P, O'Rourke D, et al. Dexamethasone potentiates the antiangiogenic activity of docetaxel in castration-resistant prostate cancer. Br J Cancer 2008;99:2054-64.

37. Bottsford-Miller JN, Coleman RL, Sood AK. Resistance and escape from anti-angiogenesis therapy: clinical implications and future strategies. J Clin Oncol 2012;30: 4026-34.

38. Ammirante M, Shalapour S, Kang Y, Jamieson CA, Karin M. Tissue injury and hypoxia promote malignant progression of prostate cancer by inducing CXCL13 expression in tumor myofibroblasts. Proc Natl Acad Sci U S A. 2014;111:14776-81.

39. James ND, Sydes MR, Clarke NW, Mason MD, Dearnaley DP, Spears MR, et al. Addition of docetaxel, zoledronic acid, or both to first-line long-term hormone therapy in prostate cancer (STAMPEDE): survival results from an adaptive, multiarm, multistage, platform randomised controlled trial. Lancet 2016;387:1163-77.

40. Jain RK. Antiangiogenesis strategies revisited: from starving tumors to alleviating hypoxia. Cancer Cell 2014;26:605-22.

41. Maxwell PJ, Gallagher R, Seaton A, Wilson C, Scullin P, Pettigrew J, et al. HIF-1 and NF-kappaB-mediated upregulation of CXCR1 and CXCR2 expression promotes cell survival in hypoxic prostate cancer cells. Oncogene 2007;26:7333-45.

42. Danza G, Di Serio C, Ambrosio MR, Sturli N, Lonetto G, Rosati F, et al. Notch3 is activated by chronic hypoxia and contributes to the progression of human prostate cancer. Int J Cancer 2013;133:2577-86.

43. Liao D, Johnson RS. Hypoxia: a key regulator of angiogenesis in cancer. Cancer Metastasis Rev 2007;26:281-90.

44. Li Z, Rich JN. Hypoxia and hypoxia inducible factors in cancer stem cell maintenance. Curr Top Microbiol Immunol 2010;345:21-30.

45. Greijer AE, van der Wall E. The role of hypoxia inducible factor 1 (HIF-1) in hypoxia induced apoptosis. J Clin Pathol 2004;57:1009-14.

46. Akech J, Wixted JJ, Bedard K, van der Deen M, Hussain S, Guise TA, et al. Runx2 association with progression of prostate cancer in patients: Mechanisms mediating bone osteolysis and osteoblastic metastatic lesions. Oncogene 2010;29:811-21.

47. Shore P. A role for Runx2 in normal mammary gland and breast cancer bone metastasis. J Cell Biochem 2005;96:484-9.

48. Pratap J, Wixted JJ, Gaur T, Zaidi SK, Dobson J, Gokul KD, et al. Runx2 transcriptional activation of indian hedgehog and a downstream bone metastatic pathway in breast cancer cells. Cancer Res 2008;68:7795-802.

49. Wai PY, Mi Z, Gao C, Guo H, Marroquin C, Kuo PC. Ets-1 and runx2 regulate transcription of a metastatic gene, osteopontin, in murine colorectal cancer cells. J Biol Chem 2006;281:18973-82.

FIGURE LEGENDS

Figure 1. OCT1002 targets prostate cancer cells in hypoxic conditions

(A) Structure of unidirectional hypoxia-activated prodrug OCT1002 and its reduction product OCT1001. (B) LNCaP-luc tumors grown in a dorsal skin flap. Images show FITC-dextran labelled tumor vasculature (green) and activated OCT1002, i.e. OCT1001 (blue); this is visible in hypoxic regions 4 hours after administration on Day 7 (middle panel) and is still present 7 days later (right panel). Untreated tumors show no auto-fluorescence (left panel). (C) Treatment of LNCaP-luc, 22Rv1 and PC3 prostate cancer cell-lines revealed no significant toxicity at concentrations of OCT1002 <1µM. (D) Treatment of LNCaP-luc cells with 1µM OCT1002 significantly decreased viability of cells grown in hypoxia (0.1% oxygen) but not in normoxia (20% oxygen). All images and blots are representative of 3 independent experiments. Data shown in graphs are mean ± SE (Student t-test p-values: *$p<0.05$, **$p<0.01$, ***$p<0.001$, ns; not significant)

Figure 2. OCT1002 targets cells in LNCaP-luc spheroids

(A) Hypoxic markers *HIF1A, IGF-1* and miR-210 in LNCaP spheroids after 10 days growth. (B) Images reveal evidence of hypoxia in LNCaP spheroids as shown by the presence of reduced OCT1002 (i.e. OCT1001). Western blots show increased HiF1α protein after 10 days growth, compared to day 7. Cycling normoxic LNCaP-luc cells are included as control. (C) Graph and representative inset images show spheroid growth is reduced by OCT1002 (1µM) alone or in combination with bicalutamide compared to vehicle (0.02% DMSO in media) or bicalutamide (13.8µM) alone. (D) Crystal violet staining of colonies formed from cell disaggregates of spheroids, treated as (C) above. (E) Annexin V/PI apoptosis assay showing that OCT1002 induces apoptosis. Data is mean ± SE from triplicate experiments (Student t-test p-values: *$p<0.05$, **$p<0.01$, ***$p<0.001$, ns; not significant)

Figure 3. OCT1002 slows LNCaP-luc tumor growth *in vivo*

(A) Graph shows tumor growth in LNCaP-luc xenograft SCID mouse implants following treatment with vehicle (0.1% DMSO in corn oil), bicalutamide (2mg/kg/day), vehicle + OCT1002 (50mg/kg administered on day 7), bicalutamide + OCT1002. (B) Representative images of *in vivo* and excised tumors; quantification of tumor weights (C) Representative images and (D) histogram showing extent

of bioluminescent metastatic LNCaP-luc cells in lungs at day 28. (Data is mean ± SE from ≥5 animals per group. 2way ANOVA with Bonferroni post-tests used to compare statistical significance between vehicle and bicalutamide treatment groups; *p<0.05, ** p<0.01, *** p<0.001 and bicalutamide and combination treatment groups; ^ p<0.05, ^^ p<0.01, ^^^ p<0.001)

Figure 4. Effect of OCT1002 on vascularisation of LNCaP-luc tumor fragments

(A) Representative images of LNCaP-Luc tumor vasculature imaged via confocal microscopy following i.v. injection of FITC-dextran prior to commencing treatment (day 0) and at day 7, 14 and 21 days post-treatment with vehicle (1% DMSO), bicalutamide (2mg/kg/day), vehicle + OCT1002 (50mg/kg administered on day 7) or bicalutamide + OCT1002. Stereological analysis was used to quantify changes in the vasculature of LNCaP xenografts on day 21 including (B) vessel branch points (C) vessel density, and (D) average vessel length. Images (10X magnification) are representative of ≥3 mice per treatment. Scale bar = 100µM. (Student t-test p-values: *p<0.05, **p<0.01, ***p<0.001, ns; not significant)

Figure 5. Gene expression induced by bicalutamide is altered by addition of OCT1002

(A) Comparison of gene expression in tumors excised on day 7, 14, 21 and 28 from mice treated daily with bicalutamide (top row) or in combination with OCT1002 (50mg/kg) on day 7 (bottom row). Data in scatterplots was generated using quantitative PCR arrays, which, were carried out on pooled RNA from tumors excised at each time-point (n≥3 per group). Gene expression changes for each treatment group were calculated relative to day 0 results. Horizontal lines show 2-fold change in expression and vertical lines display p-value of 0.05 as calculated by student *t*-test. (B) Comparison of gene changes on day 21 between vehicle, bicalutamide and bicalutamide + OCT1002 treatment groups for genes which were consistently and significantly altered between groups.

Figure 6. Up-regulation of pro-survival genes induced by bicalutamide is blocked by OCT1002

(A) Quantification of immunohistochemical staining of Ki67 and RUNX2 protein expression in LNCaP-luc tumors (data generated from ≥3 mice per treatment). Insets show RUNX2 staining (brown) present in LNCaP-luc tumors at the experimental endpoint (B) Expression of *RUNX2* and downstream targets in LNCaP-luc spheroids. Data is mean ± SE from triplicate experiments. (Student t-test p-values: *p<0.05, **p<0.01, ***p<0.001, ns; not significant) (C) Proposed hypothesis for beneficial effect of

bicalutamide and OCT1002 combination. Cells which survive the bicalutamide-induced hypoxic stress can re-populate the tumor and progress to CPRC. Addition of OCT1002 targets these cells, prevents re-establishment of tumor microvasculature, and exerts greater tumor growth control.
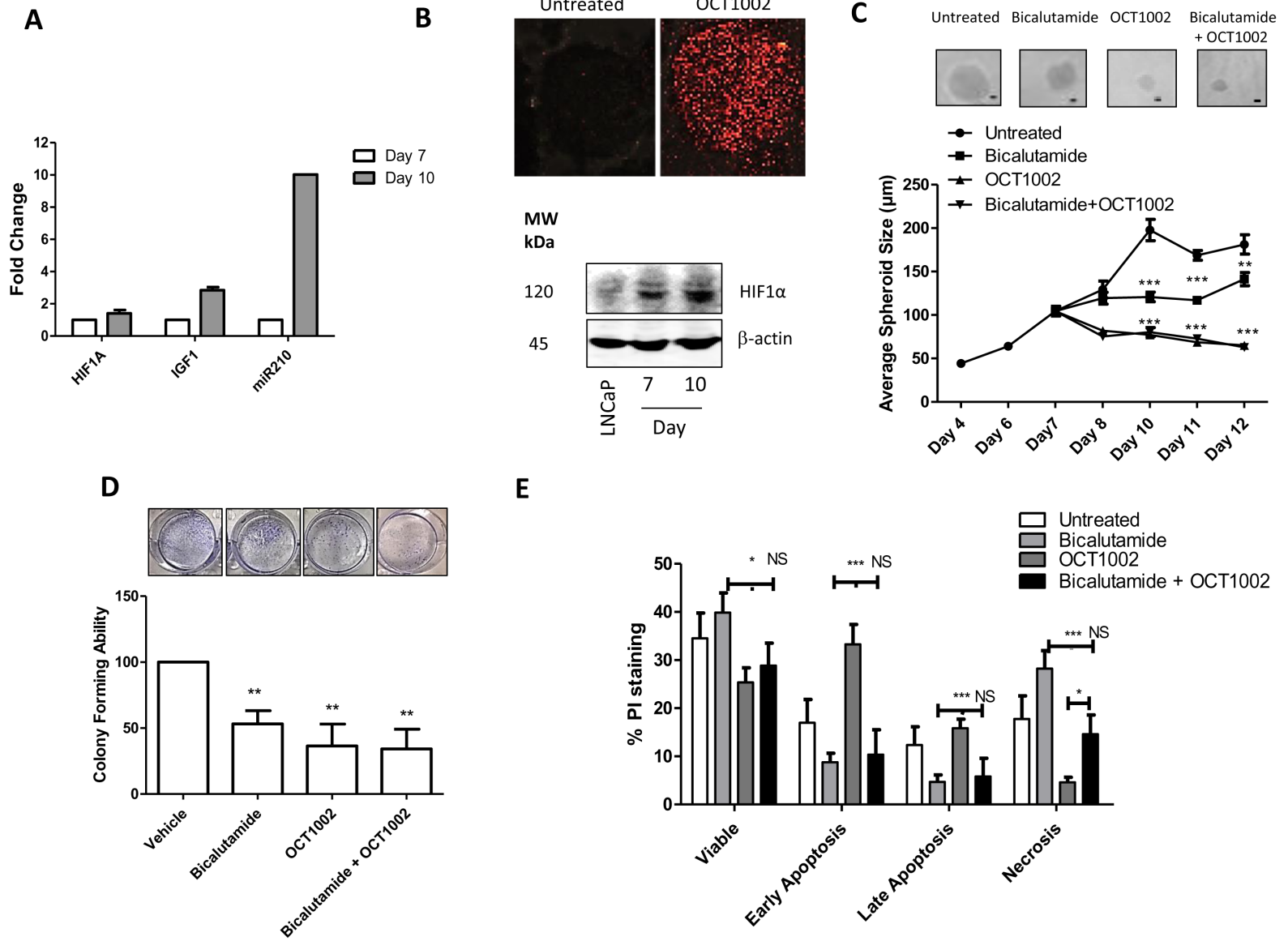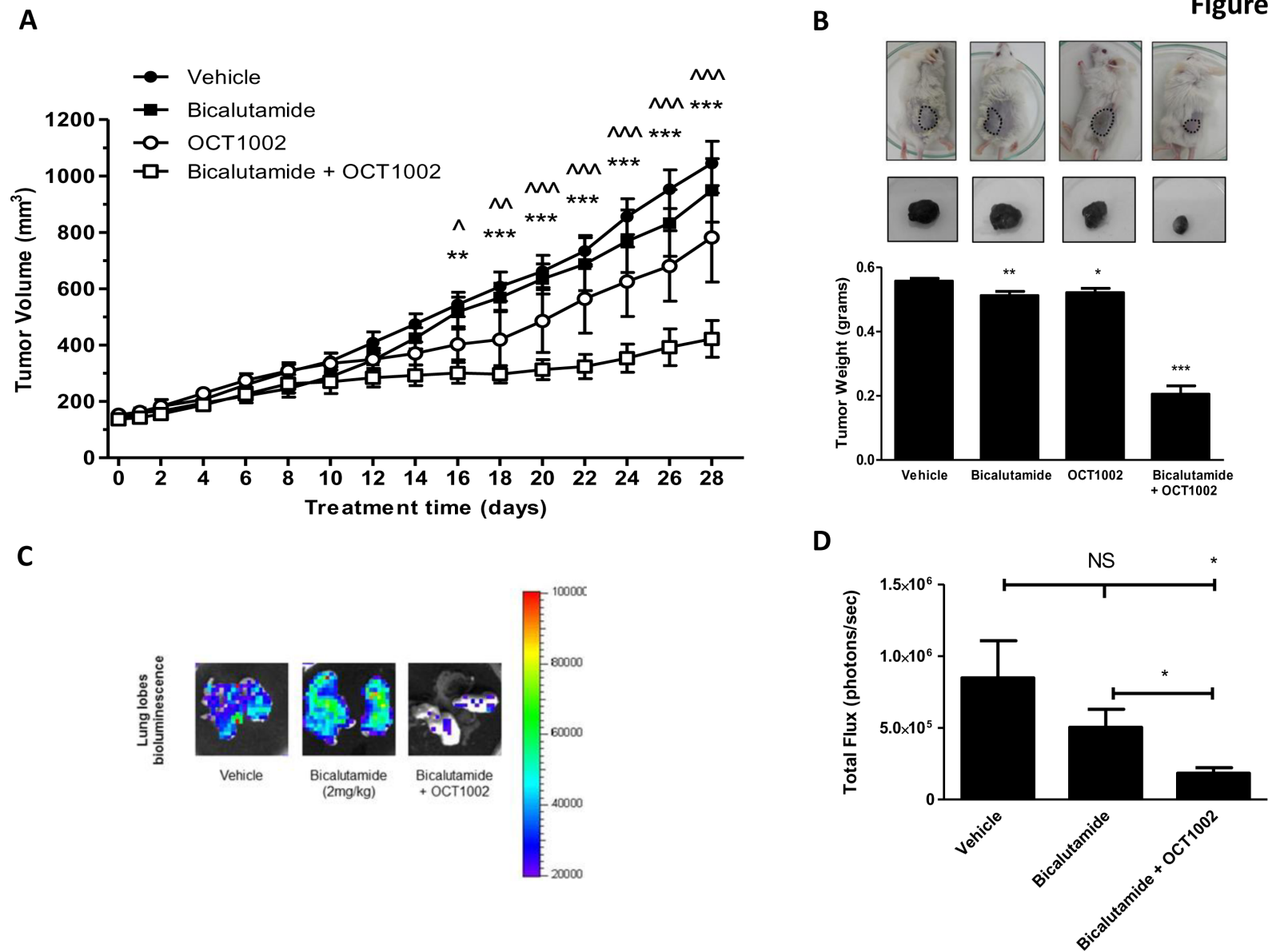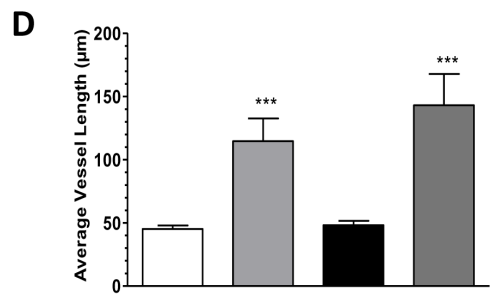
Figure 1

A

OCT1002 →(+ Hypoxia)→ OCT1001

B

Day 0   Day 7   Day 14

C

% Cell Viability vs [OCT1002] M

● 22Rv1
■ PC3
▲ LNCaP

D

48 hrs

□ Normoxic (20%)
■ Hypoxic(0.1%)

% Cell Viability

NS   ***   ***

*

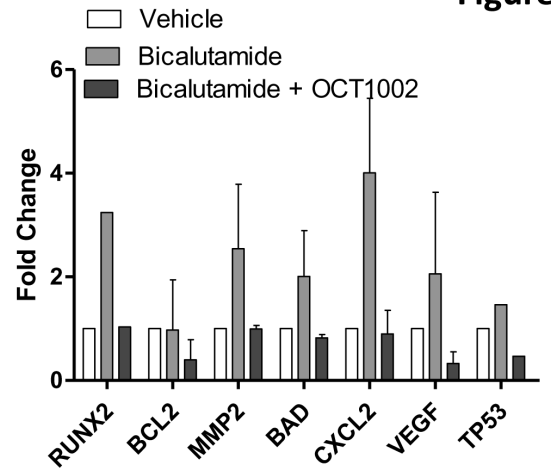Control   OCT1002 (1uM)   Control   OCT1002 (1uM)

Figure 2

A

B

C

D

E

Figure 3

Figure 4

Figure 5

A

B

Figure 6